Life Sciences 221 (2019) 47–55

Contents lists available at ScienceDirect

Life Sciences

journal homepage: www.elsevier.com/locate/lifescie

Systemic microcirculation dysfunction after low thoracic spinal cord injury in mice

Xiaochen Yuan[a,1], Qingbin Wu[a,*,1,2], Yinshan Tang[b], Yingli Jing[c,**,2], Zhigang Li[d,***,2], Ruijuan Xiu[a]

[a] Institute of Microcirculation, Key Laboratory of Microcirculation, Ministry of Health, Chinese Academy of Medical Sciences & Peking Union Medical College, Beijing 100005, China
[b] Department of Rehabilitation in Traditional Chinese Medicine, The Second Affiliated Hospital of Zhejiang University School of Medicine Hangzhou, Hangzhou 310000, China
[c] China Rehabilitation Science Institute, China Rehabilitation Research Center, Center of Neural Injury and Repair, Beijing Institute for Brain Disorders, Beijing Key Laboratory of Neural Injury and Rehabilitation, Beijing 100068, China
[d] School of Acupuncture, Moxibustion and Tuina, Beijing University of Chinese Medicine, No. 11, NorthThird Ring Road East, Chaoyang, Beijing 100029, China

ARTICLE INFO

Keywords:
Endothelial permeability
Microvascular blood flow
Peripheral blood
Cytokines
Spinal cord injury

ABSTRACT

Background: Spinal cord injury (SCI) disturbs the autonomic nervous system and induces dysfunction or failure of multiple organs. The systemic microcirculation disturbance that contributes to the complications associated with SCI remains to be clarified.

Methods: We used male mice (29–32 g) and modified weight-drop injury at T10 to evaluate the systemic microcirculation dysfunction during the first 2 weeks after SCI. We determined permeability and microvascular blood flow in several organs and evaluated their vasomotor function. We also measured circulating endothelial cells (CECs), circulating endothelial progenitor cells (CEPCs), circulating pericyte progenitor cells (CPPCs), and serum proinflammatory cytokines.

Results: The endothelial permeability of almost all organs increased after SCI. Microvascular blood flow decreased in the bladder and kidney and increased in the spleen and was accompanied by endothelial vasomotor dysfunction. SCI also induced an increase in CECs, CEPCs, and CPPCs in peripheral blood. Finally, we confirmed changes in a systemic cytokine profile (interleukin [IL]-3, IL-6, IL-10, IL-13, granulocyte colony-stimulating factor, and regulated on activation normal T cell expressed and secreted) after SCI.

Conclusions: These data indicate that a systemic microcirculation disturbance occurs after SCI. This information may play a key role in the development of effective therapeutic strategies for SCI.

1. Introduction

In addition to the primary mechanical lesion, spinal cord injury (SCI) induces secondary degeneration, which extends the tissue damage [1]. Moreover, SCI disturbs the autonomic nervous system and multiple organs[2]. These disorders, which include cognitive disorder, liver damage, kidney dysfunction, and cardiovascular effects, are commonly present in patients with SCI [3]. A great deal of evidence indicates that many factors, such as pathological connection after SCI, systemic inflammation, and immunosuppression after the injury, are responsible for the post-SCI complications [4–7]. However, it is still unclear whether a systemic microcirculation disturbance contributes to the complications associated with SCI.

The microcirculation is an important factor in the inflammatory response [8]. During inflammation, the microvasculature (arterioles, capillaries, and venules) displays characteristic phenotypic alterations that seem to increase the number of inflammatory cells in the injured tissue and segregate the lesioned region from healthy tissue and the

* Correspondence to: Q. Wu, Institute of Microcirculation, Chinese Academy Medical Sciences & Pecking Union Medical College, 5, Dong Dan San Tiao, Dongcheng District, Beijing 100005, China.
** Correspondence to: Y. Jing, No. 10, Jiao men North Road, Feng tai District, Beijing 100068, China.
*** Correspondence to: Z. Li., No. 11 NorthThird Ring Road East, Chaoyang, Beijing 100029, China.
E-mail addresses: wuqingbin@imc.pumc.edu.cn (Q. Wu), jingling1090@126.com (Y. Jing), lizhigang620@126.com (Z. Li).
[1] Xiaochen Yuan and Qingbin Wu contributed equally to the work.
[2] The authors are the co-correspondence authors of this work.

https://doi.org/10.1016/j.lfs.2019.02.010
Received 17 July 2018; Received in revised form 26 January 2019; Accepted 3 February 2019
Available online 06 February 2019
0024-3205/

systemic circulation. Various cells that normally spread in blood (leukocytes, platelets) or localize to the vessel wall (endothelial cells [ECs], pericytes) are activated in response to inflammation [9]. Microcirculation has many characteristic responses to inflammation, such as impaired vasomotor function, abnormal capillary perfusion, increased vascular permeability, mobilization and recruitment of angiogenic progenitor cells, and increased circulating ECs (CECs) [10–13]. Microcirculation alterations, especially in the early stage of SCI, might be one of the pathogenic factors involved in the injury-associated complications.

Therefore, we aimed to study microcirculatory function in SCI animal models of acute and subacute post-traumatic contusion. We determined permeability and microvascular blood flow (MVBF) and evaluated the vasomotor function of several organs. We also measured CECs, circulating endothelial progenitor cells (CEPCs), circulating pericyte progenitor cells (CPPCs), and serum proinflammatory cytokines. Evaluation of the microcirculation may suggest new therapeutic strategies for SCI-induced complications.

2. Materials and methods

2.1. Experimental animals

Eight-week-old male ICR mice were bought from the Institute of Laboratory Animal Science, Chinese Academy of Medical Sciences (CAMS) & Peking Union Medical College (PUMC). The mice were maintained at 26 °C and 38.5% humidity under a 12-h light/dark cycle (light on from 07:30 to 19:30 h).

2.2. Animal welfare

The animal experimental procedures were approved by the Experimental Animal Care and Ethics Committee of the Institute of Microcirculation, CAMS & PUMC.

2.3. Experimental design

To evaluate permeability using Evan's Blue dye, mice were divided into two groups: a sham group and an SCI group. Each group contained four subgroups ($n = 6$ each): 1 day, 3 days, 7 days, and 14 days. For the laser Doppler imaging (LDI), laser Doppler flowmetry (LDF), cytokine, and flow cytometry analyses, mice were randomly divided into two groups: a sham group and an SCI group. Each group contained four subgroups ($n = 6$ each): 1 day, 3 days, 7 days, and 14 days. To prevent potential biases in performance and detection, the people who performed the experiments, collected data, and assessed outcomes were blinded to animal groupings throughout the course of the experiments.

2.4. Creation of animal models

Animals were anesthetized using 1.5% isoflurane inhalation and underwent laminectomy at the thoracic vertebra level 10 (T10) on a thermostat-controlled heating pad in the prone position. Briefly, a laminectomy was performed at the T10 level and the spinous processes of T8 and T11 were clamped to stabilize the spine. Mice received a 50-kilodyne spinal contusion injury using the Infinite Horizons Impactor (Precision Systems & Instrumentation, Lexington, KY) [14]. Mice in the sham group only underwent the laminectomy without impact. Mice were placed in a warming chamber at approximately 40 °C until they were completely awake. Due to the neurogenic bowel and bladder after SCI, feces and urine were manually expressed. We used buprenorphine (0.05 mg/kg, intraperitoneal) immediately and every 6 h post-surgery for 1 day to reduce pain.

2.5. Assessment of microvascular penetrability

Evan's Blue leakage was evaluated as described previously [15]. Evan's Blue dye (2% (w/v) in saline; Sigma-Aldrich, St Louis, MO) was infused intraperitoneally into animals. After 3 h, mice were narcotized and transcardially infused with saline, followed by 4% paraformaldehyde. The organs, including the brain, spinal cord, spleen, testis, liver, lung, bladder, and kidney, were removed, dried, and weighed. Samples were homogenized in a 50% trichloroacetic acid solution for 3 days at room temperature and centrifuged at 10,000 $\times g$ for 10 min. The fluorescence of the supernatants was then quantified at an excitation wavelength of 620 nm and an emission wavelength of 680 nm. A standard curve with Evan's Blue dye (0 μg, 50 μg, 100 μg, 200 μg, 400 μg, 800 μg, 1600 μg, 3200 μg, and 6400 μg in trichloroacetic acid) was generated and fluorescence intensity was measured using a spectrophotometer at the above excitation and emission wavelengths. All measurements were within the range of detection established by the standard curve. The dye concentration was calculated as the ratio of absorbance relative to the amount of tissue. Dye weight of samples was recorded as μg/mg of tissue.

2.6. LDI measurement of organ blood perfusion

MVBF was examined using a Laser Doppler Line Scanner® (Moor Instruments Ltd., Axminster, UK) at a stable temperature (24 ± 1 °C) and 60% relative humidity. The mice were anesthetized and a line of 785 ± 10 nm laser light was scanned over the organs. The spleen and kidney were exposed through a paracostal incision, the brain through a scalp incision, and the bladder through a midline lower abdominal laparotomy. The bilateral testes were exteriorized through a scrotal incision. A scanning mirror along with other optics onto a 64-element linear array was used to direct the Doppler-shifted light from moving blood cells and the non-shifted light from stationary tissue in order to establish a two-dimensional color-coded perfusion image. Data were computerized and recorded as image and numerical data (perfusion units). For LDI analysis, five flux images were obtained through continuous scanning. Thereafter, in moorLDI Image Review (version 5.3; Moor Instruments Ltd.), the images were averaged to minimize any disturbance caused by movements [16].

2.7. Detection of organ vasomotion and spectral analysis of LDF signals

After measurement of blood perfusion, vasomotion was detected using a dual-channel laser Doppler monitor instrument (moorVMS-LDF2, Moor Instruments, Ltd.) and a fiberoptic probe (Moor Instruments Ltd.) with a calculated penetration depth of 2.5 mm. The electrode was placed within 1 mm of the detection site. After each run, the probes were replaced to shun additive effects and partial exhaustion of contractile and relaxing ability.

A specific device containing colloidal latex particles was used to calibrate data before each test session. The Brownian motion of these particles provided the normalized values. The LDF signal was continuously documented by an interfaced computer running Moor software for Windows (moorVMS-PC version 2.0, Moor Instruments Ltd.) as previously described [16]. Briefly, as for the analysis of LDF, 5-min consecutive data were filtered by a built-in noise filter in the software to remove any noise spikes and frequencies above 10 Hz, which were used for subsequent wavelet analysis. The wavelet analysis was performed by means of the Moor software. A three-dimensional plot was produced from the wavelet transformations of perfusion signals, which connected representations of vasomotor outputs in time and frequency domains. Then, the three-dimensional plot was projected in two dimensions as the average over time (Fig. 1A). According to previous studies [17–19], 0.01–5.00 Hz was detected and slower contributions (0.01–0.25 Hz) were recognized as being caused by endothelial factors. The relative value of endothelial factors was recorded as the ratio between the

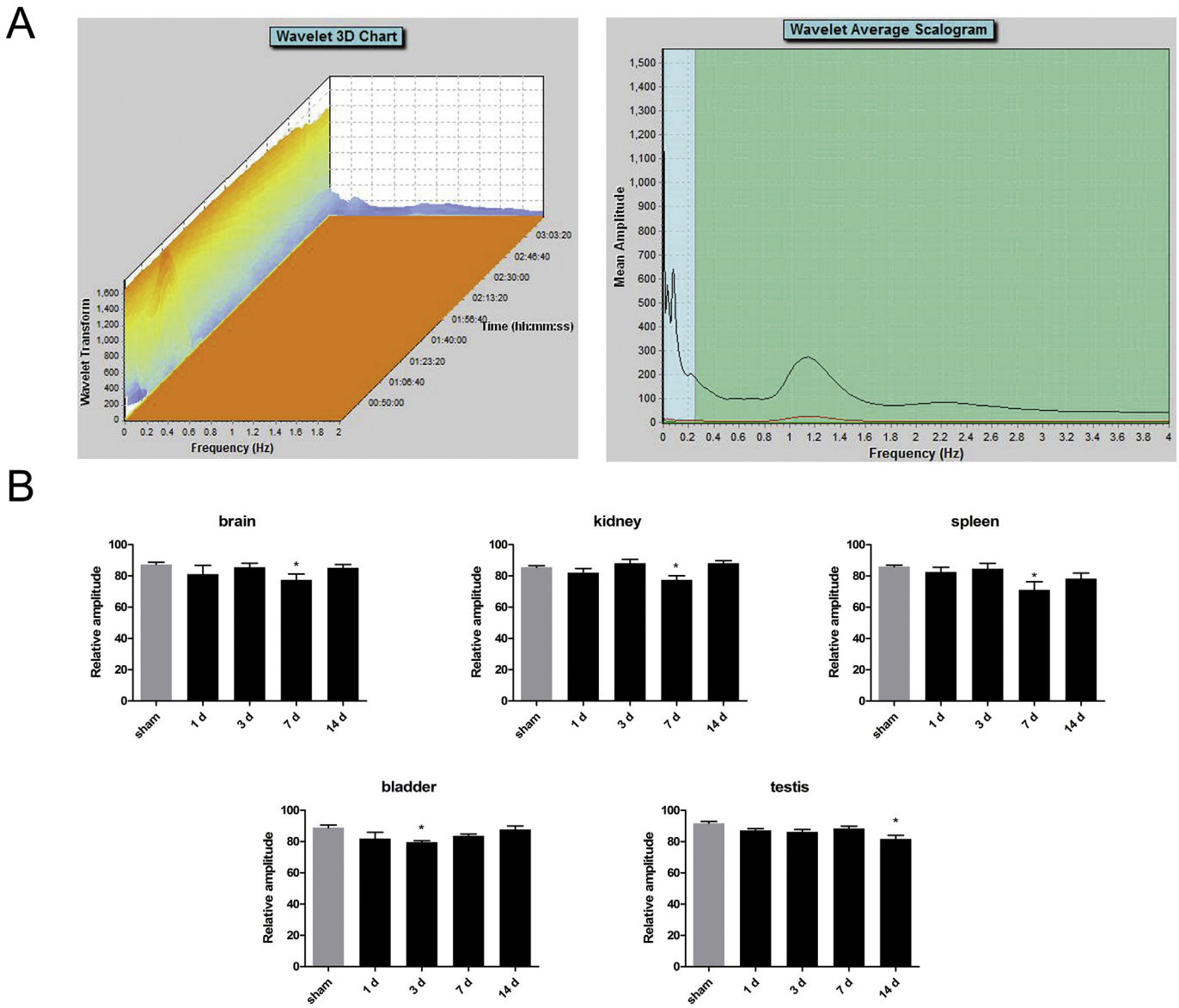

Fig. 1. Spectral analysis of endothelial factors. A, Corresponding vasomotor amplitude during the study period. B, Values of the relative amplitudes of the oscillatory LDF signal for endothelial factors. $n = 6$ in each group. *P $<$ 0.05 compared with the sham group.

endothelial amplitude value and the sum amplitudes for the total frequency range.

2.8. Flow cytometry

Blood was collected by retro-orbital puncture and anticoagulated using ethylenediaminetetraacetic acid. Immunostaining was performed according to previous methods immediately after sample collection [20–22]. Briefly, 200 μL blood was collected in a tube and centrifuged at 500 ×*g* for 10 min. We discarded the upper plasma phase and resuspended the lower phase in cold phosphate-buffered saline (PBS) and incubated it on ice for 30 min. Then, FcR-blocking agent was added at a concentration of 1 μg/mL and the tubes were incubated on ice for 10 min. Samples and the fluorescence-minus-one (FMO) control were marked using antibodies and fluorescence dye. To detect CPPCs, the following monoclonal antibodies directly labeled with fluorochromes were used: CD140b-PE, CD45-APC, and CD31-PE/Cy7 (BioLegend, San Diego, CA) and the Syto16-FITC nuclear stain (Invitrogen, Carlsbad, CA). To detect CEPCs and CECs, we used Flk-1-PE, CD117-PE/Cy7 (BioLegend), CD45-APC, and Syto16-FITC. After incubation, 2-mL RBC Lysis Buffer (Thermo scientific, Waltham, MA) was added to lyse red blood cells according to the manufacturer's specification. The lysis buffer was diluted with 2 mL PBS to stop the reaction. The cells were centrifuged at 300 ×*g* and resuspended in 200 μL PBS. For absolute counts, the reagent 123count eBeads, which contains approximately 1000 beads/μL, was used. We added 50 μL of beads into each tube and briefly vortexed the tube before collection to ensure equal distribution of cells and beads.

Before analysis, the residual cells in the flow cytometer were thoroughly removed. Samples were analyzed using an Accuri C6 Flow Cytometer and Accuri CFlow analysis software (version 1.0.264.15) at a medium flow rate ($<$ 3000 events per second) using an FSC-H threshold of 550,000 to avoid debris and electronic noise. In each analysis, 1000,000 total events were gathered. For each blood sample, FMO-matched controls were analyzed to set the appropriate regions.

CECs were positive for Syto16 (DNA) and Flk-1 (EC marker) and negative for CD117 (progenitor marker) and CD45 (hematopoietic marker). CEPCs were positive for Syto16 (DNA), CD117, and Flk-1 and negative for CD45. CPPCs were positive for Syto16 (DNA) and CD140b and negative for CD45 and CD31 (EC marker) (Fig. 2).

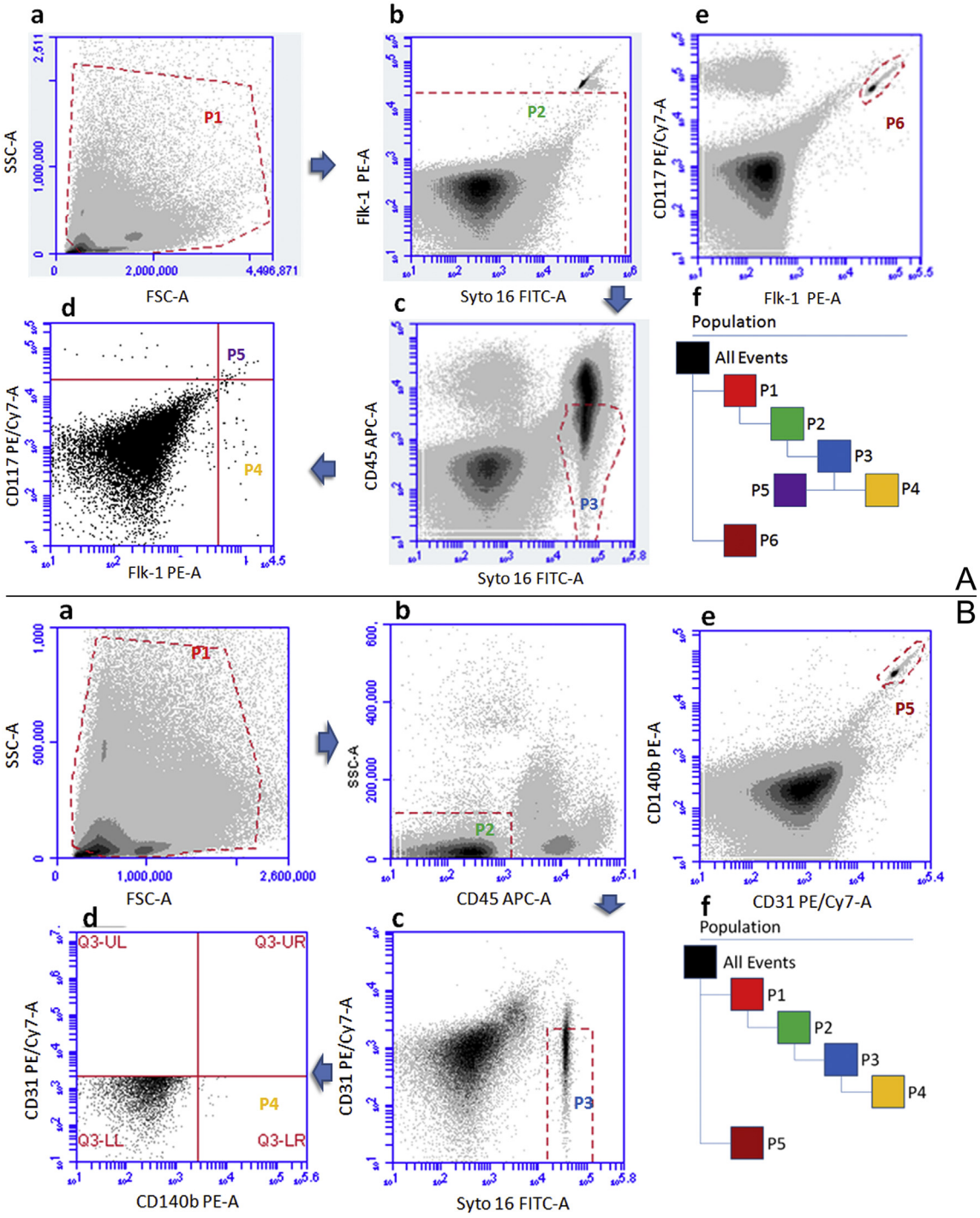

Fig. 2. Detection of circulating EPCs, ECs, and PPCs. A, Analytical strategy for CECs and EPCs. All leukocytes were first gated on a FSC/SSC dot plot as P1 (a). This P1 population was displayed on a Syto16/Flk-1 dot plot and the events showing a natural distribution were gated as P2 (b). The P2 cell set was displayed on a CD45/Syto16 dot plot following gating of the CD45-Syto16+ events as P3 (c). The CD45-Syto16+ events were displayed on a Flk-1/CD117 dot plot, and the cutoffs were gated for Flk-1 + CD117+ events as P5 for EPCs and for Flk-1 + CD117- events as P4 for CECs (d). For bead counting, the bead region was gated as P6 (e). Population hierarchy (f). Analytical strategy for CECs and EPCs. CEC absolute count = [Cell Count (# of cells in P4] × Bead Volume (50 μL)]/[Bead Count (# of events in P6) × Initial Volume (200 μL)] × Bead Concentration. EPC absolute count = [Cell Count (# of cells in P5) × Bead Volume (50 μL)]/[Bead Count (# of events in P6) × Initial Volume (200 μL)] × Bead Concentration. B, Analytical strategy for PPCs. All leukocytes were first gated on a FSC/SSC dot plot as P1 (a). This P1 population was displayed on a SSC/CD45 dot plot and the CD45 events were gated as P2 (b). The P2 cell set was displayed on a CD31/Syto16 dot plot following gating of the CD31-Syto16+ events as P3 (c). Finally, the CD31-Syto16+ events were displayed on a CD31/CD140b dot plot with the cutoff for CD140b + events as P4 (d). For bead counting, the bead region was gated as P5 (e). Population hierarchy (f). Analytical strategy for PPCs. PPC absolute count = [Cell Count (# of cells in P4) × Bead Volume (50 μL)]/[Bead Count (# of events in P5) × Initial Volume (200 μL)] × Bead Concentration.

According to the instructions for the 123count eBeads system and other references, the absolute enumeration of cells was regarded as the concentration of the original blood sample in the tube.

2.9. Measurement of cytokine profiles

A magnetic bead-based multiplex assay system that can detect and quantify multiple cytokines from a single sample of plasma was used to analyze cytokines. A mouse cytokine 23-plex assay (Bio-Plex Pro Mouse Cytokine 23-plex, #M60009RDPD) was used to simultaneously measure the levels of 23 cytokines (eotaxin, granulocyte colony-stimulating factor [G-CSF], granulocyte-macrophage colony-stimulating factor, interferon γ, interleukin [IL]-1β, IL-1α, IL-2, IL-3, IL-4, IL-5, IL-6, IL-9, IL-10, IL-12p40, IL-12p70, IL-13, IL-17A, Keratinocyte chemoattractant, monocyte chemotactic protein-1, macrophage inflammatory protein [MIP]-1α, MIP-1β, regulated on activation normal T cell expressed and secreted [RANTES], and tumor necrosis factor). All standards, reagents, and samples were prepared according to the manufacturer's instructions. We analyzed plasma aliquots (50 μL), with a minimum of 50 beads acquired per analyte. The plates were analyzed with a multiplexing diagnostic instrument (Bio-Plex 200; Bio-Rad, Hercules, CA). The fluorescent data of each cytokine were obtained using the manufacturer's software (Bio-Plex Manager 6.1; Bio-Rad). The standard curve of each analysis was produced using standards supplied by the manufacturer.

2.10. Statistical analysis

Data are expressed as the mean ± standard error of the mean (SEM) and were analyzed using SPSS version 17.0 statistic software (SPSS Inc., Chicago, IL). Differences between two groups were determined by Student's *t*-tests. One-way analysis of variance followed by post-hoc Tukey's analysis was used to compare three or more groups. Results were considered significant at $P < 0.05$.

3. Results

3.1. Microvascular permeability of organs after SCI

It is crucially important to investigate vascular barrier permeability in order to understand the vasculature disruption after SCI. Here, we successfully established SCI model (Figs. 3 and 4). Then we examined the dynamic changes in microvascular permeability over time, from 1 day post-injury (dpi) to 14 dpi (Fig. 5). During our observation period, the blood–spinal cord barrier was maximally damaged at 1 dpi and appeared to be restored at 7 dpi and 14 dpi. The blood–brain barrier was disrupted from 3 dpi until 14 dpi. When compared with the sham group, the permeability of the blood–testes barrier in the SCI group increased at 3 dpi, peaked at 7 dpi, and was still higher at 14 dpi. The microvascular permeability of the spleen and liver was markedly higher in the SCI group than in the sham group at 1 dpi after injury and gradually increased from 1 dpi to 14 dpi. The microvascular permeability of the lung and kidney in the SCI group at 1 dpi was increased when compared with that in the sham group; this increase persisted until 14 dpi. The microvascular permeability of the bladder was higher in the SCI group than in the sham group at 7 and 14 dpi.

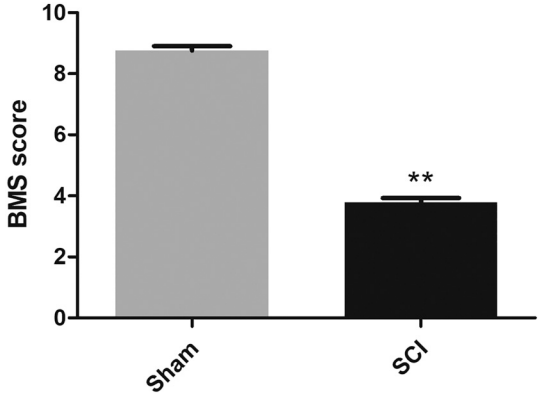

Fig. 4. Basso mouse scale (BMS) of sham and SCI mice at 14 days. $n = 6$ in each group. **P < 0.01 compared with the sham group.

3.2. Organ blood perfusion and spectral analysis of endothelial factors related to vasomotion after SCI

SCI was responsible for the alterations in the MVBF (Fig. 6). Clear differences were observed in most tissues between the sham and injured groups, except the brain and testes. However, the MVBF was not altered in the same pattern in these organs. In the kidney, the MVBF was significantly decreased at 14 dpi. In the bladder, the MVBF was maximally decreased at 1 dpi, which lasted until 14 dpi. In the spleen, the MVBF peaked at 3 dpi and then returned to baseline levels. Additionally, LDF investigation of organ microcirculation was performed via spectral analysis of organ blood flow oscillation (Fig. 1). The data showed that the relative values of endothelial factors decreased in the bladder at 3 dpi and in the spleen, brain, testes, and kidney at 7 dpi, suggesting that systemic and local microvascular disturbances after SCI might be related to alterations in endothelial function.

3.3. Detachment of ECs and mobilization of CEPCs and CPPCs after SCI

To investigate whether SCI triggers the production of CECs, CEPCs, and CPPCs in the peripheral blood, flow cytometry was used to determine the numbers of CECs, CEPCs, and CPPCs in mice at 1, 3, 7, and 14 dpi (Fig. 7). The number of CECs was much higher in SCI mice than in the sham group at 3 and 7 dpi. The number of CEPCs in SCI mice peaked at 3 dpi and gradually reduced at 7 and 14 dpi. The kinetics of CEPCs were similar to those of CPPCs. The numbers of CEPCs and CPPCs were unaltered at 1 dpi in the two groups. The numbers of CEPCs

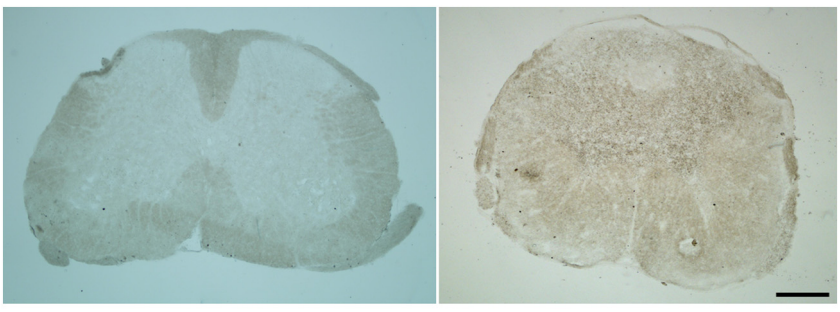

Fig. 3. Histological images of sham and SCI mice at 14 days. Scale bar = 200 μm.

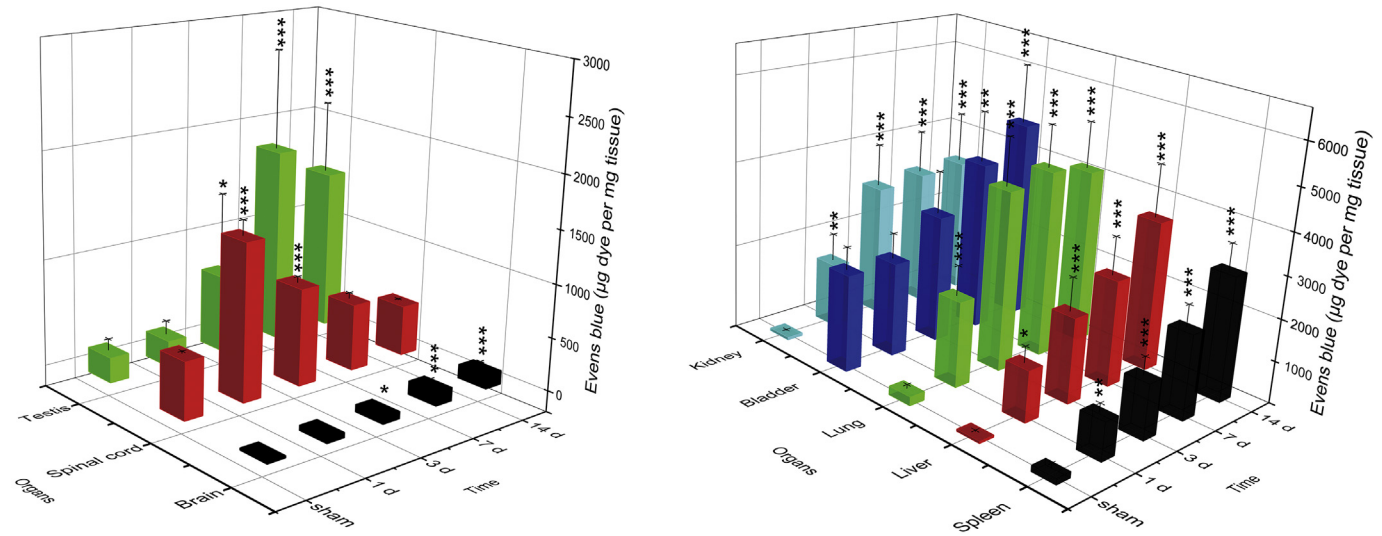

Fig. 5. Temporal disruption of the microvascular barrier of organs as evaluated using Evan's Blue spectrophotometry. Quantification of the amount of Evan's Blue in different organs and tissues. n = 6 in each group. *P < 0.05, **P < 0.01, ***P < 0.001 compared with the sham group.

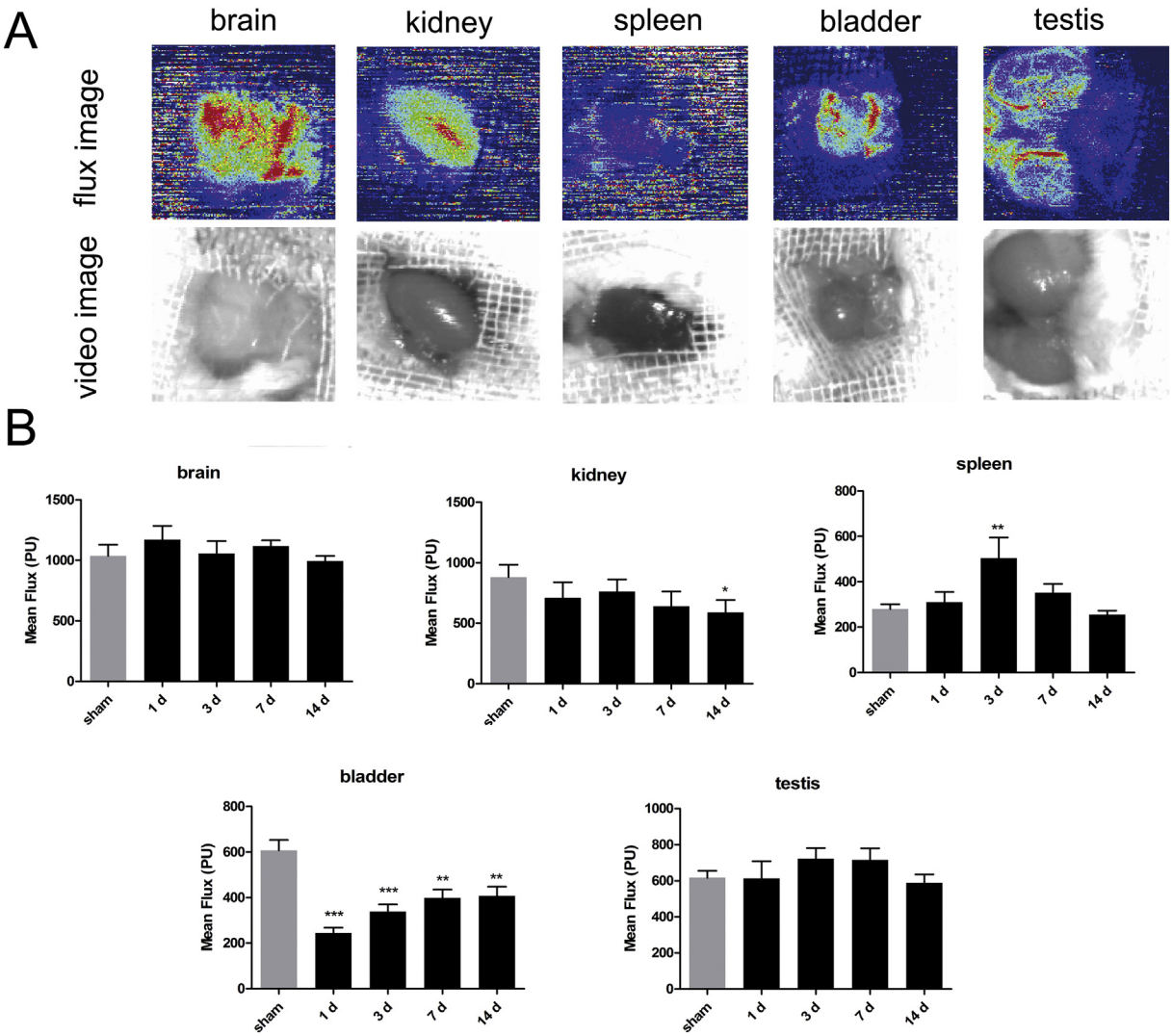

Fig. 6. Organ blood perfusion. Blood flow of organs was detected using a Laser Doppler Line Scanner. A, Video and flux images of several organs. B, Quantification of blood flow. n = 6 in each group. *P < 0.05, **P < 0.01 compared with the sham group.

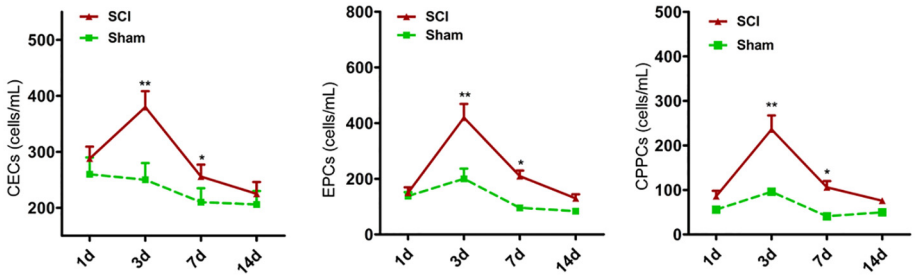

Fig. 7. Numbers of circulating EPCs, ECs, and PPCs in peripheral blood after SCI. Data are presented as the mean ± SEM. n = 6 in each subgroup. *P < 0.05 compared with the sham group on the same day.

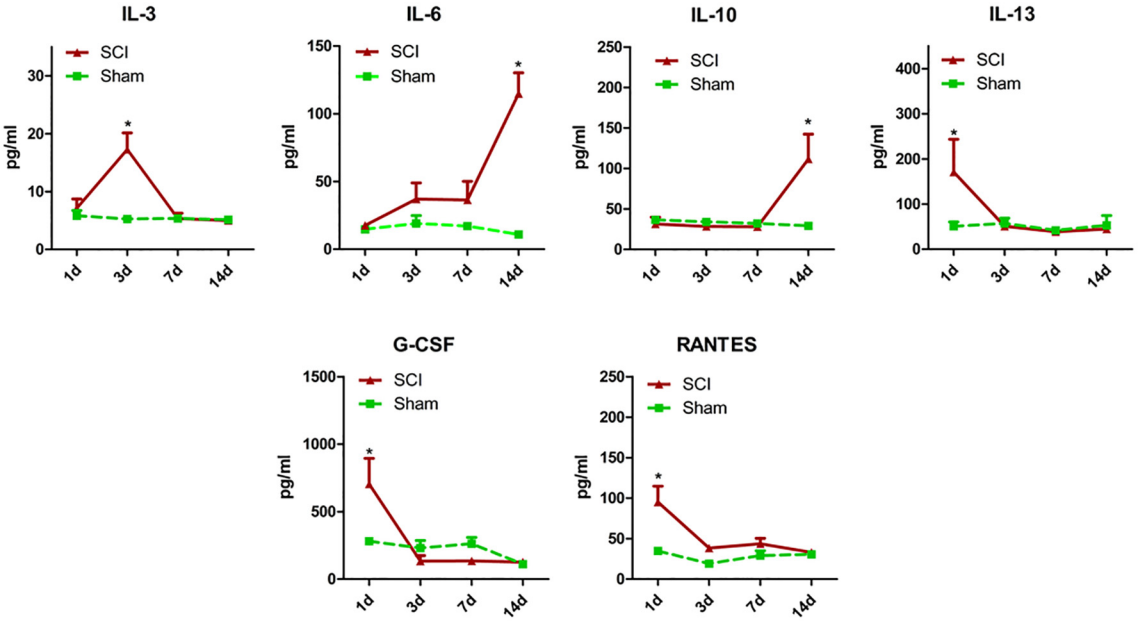

Fig. 8. Concentrations of chemokines and inflammatory cytokines in plasma. Quantitative analysis of IL-3, IL-10, IL-13, G-CSF, and RANTES levels in different groups. Data are presented as the mean ± SEM. n = 6 in each subgroup. *P < 0.05 compared with the sham group on the same day.

and CPPCs were also significantly higher in SCI mice than in the sham group at 3 and 7 dpi. The numbers of CEPCs and CPPCs in SCI mice peaked at 3 dpi and were moderately decreased at 7 and 14 dpi.

3.4. Plasma levels of chemokines and inflammatory cytokines in mice with SCI

The levels of 23 cytokines were analyzed using a multiplex enzyme immunosorbent assay in the plasma after injury (Fig. 8). The levels of plasma IL-10 and IL-6 at 14 dpi, IL-3 at 3 dpi, and IL-13 at 1 dpi were clearly higher in the SCI group than in the sham group. The level of plasma G-CSF was significantly increased at 1 dpi but returned to baseline from 3 to 14 dpi. The trend of RANTES was similar to that of G-CSF at 3 dpi.

4. Discussion

This study evaluated systemic microcirculation function after SCI in mice during the first 2 weeks after injury (acute and subacute periods). We found increased endothelial permeability in almost all organs after SCI. We observed decreased MVBF in the bladder and kidney and increased flow in the spleen, as well as endothelial vasomotor dysfunction. We found that SCI increased the levels of CECs, CEPCs, and CPPCs in the peripheral blood. Finally, we studied the changes in the systemic cytokine profile related to microcirculation disorders after SCI.

The endothelium forms the innermost lining of blood vessels. Maintenance of the barrier characteristics of the endothelium is crucial for physiological function [9,23–25]. Endothelial barrier function mainly relies on adherens junctions, tight junctions, and gap junctions between ECs [26]. After stimulation by intrinsic and extrinsic proinflammatory mediators, inter-endothelial junctions open to allow paracellular fluid passage. Endothelial barrier disruption and hyperpermeability contribute to the pathogenesis of various acute and chronic inflammatory diseases. In this study, most organs showed increased endothelial permeability from 1 day after injury until 14 days. In addition to the blood–spinal cord barrier and blood–brain barrier in the central nervous system, peripheral organs have other similar barriers, such as the blood–testes barrier and blood–spleen barrier. Increased permeability of the endothelial barrier can cause tissue edema, inflammatory cell infiltration, and dysfunction of these organs and result in the clinical complications of SCI, such as pulmonary edema, liver edema, immune abnormalities, and renal dysfunction [6].

Most studies of the microcirculation after SCI have focused on the spinal cord itself [27,28]. An altered MVBF in other organs after SCI has not been well studied. Better understanding of the MVBF in specific organs is needed because changes in tissue perfusion may be related to the pathophysiology of organ dysfunction. Here, we revealed the time course of changes in the organ system microcirculation after acute SCI at low thoracic levels by LDI and spectral analysis. LDI has lower spatial changeability than LDF and can provide 2D image-mapping of organ perfusion [29]. The MVBF is considered the most important hemodynamic variable in maintaining tissue perfusion. Systemic and metabolic

disturbances after SCI could be related to organ-specific changes in the MVBF that cause ischemia and/or hyperemia and possible organ damage. The observed decrease in the MVBF in the bladder might be because high pressure on the bladder wall blocks blood flow. In addition, there was a gradual decrease in the MVBF of the kidney over time, which might be related to increased renal blood flow resistance caused by urinary retention. Additionally, the MVBF of the spleen was increased at 3 dpi, and we speculated that this increase might be associated with immunological stress and organ-specific vascular responses. The MVBF is mainly controlled by the constriction and dilatation of precapillary sphincters, depending on neuromodulation and local factors. Regulatory mechanisms mainly involve the release of endothelial vasoactive mediators and autonomic feedback. SCI could cause an imbalance among vasoregulatory compounds that is dependent on both systemic and intrinsic autoregulatory mechanisms.

LDF signals are usually analyzed by wavelet analysis [30]. The frequency spectrum can fall into a predefined range of interest in order to discard signals at higher or lower frequencies and analyze the events happening at the frequencies of interest. For mice, slower frequencies (< 0.25 Hz) are caused by endothelial factors (without nervous regulation) [31,32]. Here, we mainly observed the effect of SCI on endothelium factors related to vasomotion. The results indicated that the ability of the endothelium to regulate vascular activity was interrupted after SCI.

Evidence indicates that the number of CECs reflects endothelial damage [24]. CECs are regarded as mature cells that are shed from the intimal monolayer after endothelial damage [33]. The number of CECs is elevated in states of vascular remodeling and injury [34,35]. In this study, there was a significantly higher number of CECs in SCI mice at 3 and 7 dpi. There may be two possible reasons for this finding. First, in the traumatized spinal cord, vascular injury might result in endothelial cell shedding. Second, prolonged systemic inflammation, ROS activity, cytokines, and tissue proteases that disrupt the integrity of integrin and adhesion of cadherin in ECs might also cause shedding of ECs from the blood vascular system. In contrast, CEPCs, mainly derived from the bone marrow, are considered to participate in vascular regeneration and renewal[36,37] and may represent a type of cells that are key to tissue repair.

Here, we determined that acute SCI increased the number of CEPCs, which is in accordance with recent animal studies showing that the number of CEPC colonies from circulating mononuclear cells increased after SCI and peaked at 3 dpi [38,39]. Successful revascularization of injury tissue relies on the formation of new vessels and their stabilization and maturation via the recruitment of support cells. Indeed, increasing evidence shows the existence of circulating progenitors for other phenotypes besides CEPCs. Indeed, CPPCs in the bloodstream have been described [40]. In this study, we observed that acute SCI increased the numbers of CPPCs. The mode of circulating EPC kinetics after SCI was mainly similar to those of CPPCs. Work has shown that bone marrow-derived EPCs may contribute to tissue repair by augmenting neovascularization and astrogliosis following SCI [41]. However, there is no research on pericyte progenitor transplantation after SCI. This may be a future research direction for us.

SCI is triggered by primary damage, such as mechanical injury of the spinal cord, leading to progressive tissue loss, and by secondary damage, involving blood vessel dysfunction and inflammation [42,43]. We speculated that the dysfunction of the endothelial barrier might be related to a systemic inflammatory reaction caused by SCI. Based on the data from this study, elevated plasma levels of cytokines, including IL-3, IL-6, IL-10, IL-13, G-CSF, and RANTES, might affect endothelial function. IL-6 is a multi-functional cytokine regarded as a primary mediator of the acute phase response [44]. Several types of immune cells and capillary components, including ECs and pericytes, produce IL-6 [45–48]. IL-13 is a cytokine produced by T cells that can promote the accumulation of eosinophils during inflammatory reactions [49]. RANTES is a chemoattractant and immunoregulatory molecule that is secreted by some types of cells such as macrophages, ECs, and pericytes [50]. Increased expressions of IL-6, IL-13, and RANTES after SCI likely come from resident and infiltrating immune cells, in addition to the vascular cells themselves. Besides these factors that disrupt the endothelial barrier, some factors exerting protective effects on the endothelium appeared in the plasma, including IL-10 and G-CSF. IL-10 from activated monocytes/macrophages and T cells exerts immunosuppressive and anti-inflammatory effects [51,52]. G-CSF can increase the growth capacity of ECs [53] and protect them against injury induced by various pathological stimuli [54,55]. After SCI, because both protective and destructive cytokines were simultaneously activated, further research should examine whether the destructive cytokines dominated and resulted in the endothelial dysfunction of multiple organs.

Although permeability and blood flow are two largely independent indicators, they can also affect each other. For example, endothelial damage caused by tissue ischemia-reperfusion leads to an increase in permeability. Enhanced permeability may affect the ability of the endothelium to regulate vascular activity. Permeability is associated with the stimulation of multiple inflammatory factors and blood flow is regulated by the local metabolism and innervation. The systemic inflammatory response caused by SCI stimulates ECs, causing disruption of the EC barrier and increased permeability. The sympathetic denervation caused by SCI may lead to dysregulation of organ blood flow. However, the changes in the MVBF presented here and the wavelet analysis suggest that local factors are also important.

5. Conclusion

The results of this study remind us that microcirculation disorders should be tackled in order to avoid secondary complications after SCI. Identification of the microcirculation risk of organ injury would allow for the establishment of diagnostic and therapeutic strategies. However, in-depth research is needed to identify the mechanisms underlying the MVBF disturbances and establish more effective physiological hemodynamic management after SCI.

Abbreviations

SCI	spinal cord injury
ECs	endothelial cells
MVBF	microvascular blood flow
CEPCs	circulating endothelial progenitor cells
CPPCs	circulating pericyte progenitor cells
LDI	laser Doppler imaging
LDF	laser Doppler flowmetry
PBS	phosphate-buffered saline
FMO	fluorescence-minus-one
RANTES	regulated on activation normal T cell expressed and secreted
SEM	standard error of the mean

Acknowledgements

This study was supported by the National Natural Youth Science Foundation of China (No. 81603678), the innovation fund of the Chinese Academy of Medical Sciences and Peking Union Medical College (Nos. 3332014006 and 3332015123), the Special Fund for Basic Scientific Research of the Central Public Research Institutes (Nos. 2016CZ-1 and 2018CZ-8), and the CAMS Initiative for Innovative Medicine (CAMS-I2M) (No. 2016-I2M-3-006).

Author contributions

Substantial contributions to the conception or design of the work; or the acquisition, analysis, or interpretation of data for the work: XCY and QBW.

Drafting the work or revising it critically for important intellectual content: QBW, YST and YLJ.

Final approval of the version to be published: All authors.

Agreement to be accountable for all aspects of the work in ensuring that questions related to the accuracy or integrity of any part of the work are appropriately investigated and resolved: ZGL and RJX.

Disclosure statement

The authors have no conflicts of interest to declare.

References

[1] J.D. Balentine, Pathology of experimental spinal cord trauma. II. Ultrastructure of axons and myelin, Lab. Investig. 39 (1978) 254–266.
[2] D.M. Stein, J. Menaker, K. McQuillan, C. Handley, B. Aarabi, T.M. Scalea, Risk factors for organ dysfunction and failure in patients with acute traumatic cervical spinal cord injury, Neurocrit. Care. 13 (2010) 29–39.
[3] X. Sun, Z.B. Jones, X.M. Chen, L. Zhou, K.F. So, Y. Ren, Multiple organ dysfunction and systemic inflammation after spinal cord injury: a complex relationship, J. Neuroinflammation 13 (2016) 260.
[4] A.K. Kesani, J.C. Urquhart, N. Bedard, P. Leelapattana, F. Siddiqi, K.R. Gurr, et al., Systemic inflammatory response syndrome in patients with spinal cord injury: does its presence at admission affect patient outcomes? Clinical article, J. Neurosurg. Spine 21 (2014) 296–302.
[5] J.M. Schwab, Y. Zhang, M.A. Kopp, B. Brommer, P.G. Popovich, The paradox of chronic neuroinflammation, systemic immune suppression, autoimmunity after traumatic chronic spinal cord injury, Exp. Neurol. 258 (2014) 121–129.
[6] R. Sweis, J. Biller, Systemic complications of spinal cord injury, Curr. Neurol. Neurosci. Rep. 17 (2017) 8.
[7] Q. Wu, Y. Jing, X. Yuan, X. Zhang, B. Li, M. Liu, et al., Melatonin treatment protects against acute spinal cord injury-induced disruption of blood spinal cord barrier in mice, J. Mol. Neurosci. 54 (2014) 714–722.
[8] J.R. Lindner, M.P. Coggins, S. Kaul, A.L. Klibanov, G.H. Brandenburger, K. Ley, Microbubble persistence in the microcirculation during ischemia/reperfusion and inflammation is caused by integrin- and complement-mediated adherence to activated leukocytes, Circulation 101 (2000) 668–675.
[9] J.S. Pober, W.C. Sessa, Evolving functions of endothelial cells in inflammation, Nat. Rev. Immunol. 7 (2007) 803–815.
[10] T. Asahara, A. Kawamoto, H. Masuda, Concise review: circulating endothelial progenitor cells for vascular medicine, Stem Cells 29 (2011) 1650–1655.
[11] J.M. Hill, G. Zalos, J.P.J. Halcox, W.H. Schenke, M.A. Waclawiw, A.A. Quyyumi, et al., Circulating endothelial progenitor cells, vascular function, and cardiovascular risk, N. Engl. J. Med. 348 (2003) 593–600.
[12] T.W. Secomb, A.R. Pries, The microcirculation: physiology at the mesoscale, J. Physiol. Lond. 589 (2011) 1047–1052.
[13] X. Shu, TCt Keller, D. Begandt, J.T. Butcher, L. Biwer, A.S. Keller, et al., Endothelial nitric oxide synthase in the microcirculation, Cell. Mol. Life Sci. 72 (2015) 4561–4575.
[14] X.C. Yuan, P. Wang, H.W. Li, Q.B. Wu, X.Y. Zhang, B.W. Li, et al., Effects of melatonin on spinal cord injury-induced oxidative damage in mice testis, Andrologia 49 (2017).
[15] S. Echeverry, X.Q. Shi, S. Rivest, J. Zhang, Peripheral nerve injury alters blood-spinal cord barrier functional and molecular integrity through a selective inflammatory pathway, J. Neurosci. 31 (2011) 10819–10828.
[16] X. Yuan, Q. Wu, F. Shang, B. Li, M. Liu, B. Wang, et al., A comparison of the cutaneous microvascular properties of the spontaneously hypertensive and the Wistar-Kyoto rats by spectral analysis of laser Doppler, Clin. Exp. Hypertens. (2018) 1–11.
[17] Z. Li, E.W. Tam, A.F. Mak, R.Y. Lau, Wavelet analysis of the effects of static magnetic field on skin blood flowmotion: investigation using an in vivo rat model, In Vivo. 21 (2007) 61–68.
[18] A.Y. Neganova, D.D. Postnov, O. Sosnovtseva, J.C. Jacobsen, Rat retinal vasomotion assessed by laser speckle imaging, PLoS One 12 (2017) e0173805.
[19] A.N. Pavlov, O.V. Semyachkina-Glushkovskaya, Y. Zhang, O.A. Bibikova, O.N. Pavlova, Q. Huang, et al., Multiresolution analysis of pathological changes in cerebral venous dynamics in newborn mice with intracranial hemorrhage: adrenorelated vasorelaxation, Physiol. Meas. 35 (2014) 1983–1999.
[20] D.G. Duda, K.S. Cohen, D.T. Scadden, R.K. Jain, A protocol for phenotypic detection and enumeration of circulating endothelial cells and circulating progenitor cells in human blood, Nat. Protoc. 2 (2007) 805–810.
[21] P. Mancuso, P. Antoniotti, J. Quarna, A. Calleri, C. Rabascio, C. Tacchetti, Validation of a standardized method for enumerating circulating endothelial cells and progenitors: flow cytometry and molecular and ultrastructural analyses (vol 15, pg 267, 2009), Clin. Cancer Res. 21 (2015) (2652-).
[22] X.C. Yuan, Q.B. Wu, H.W. Li, B.W. Li, R.J. Xiu, Absolute circulating pericyte progenitor cell counts in mice by flow cytometry: comparison of 2 single-platform technologies, Int. J. Biol. Markers 30 (2015) (E434-E8).
[23] W.C. Aird, Phenotypic heterogeneity of the endothelium I. Structure, function, and mechanisms, Circ. Res. 100 (2007) 158–173.
[24] W.C. Aird, Endothelial cell heterogeneity, Cold Spring Harb. Perspect. Med. 2 (2012).
[25] A. Chavez, M. Smith, D. Mehta, New insights into the regulation of vascular permeability, Int. Rev. Cell Mol. Biol. 290 (2011) 205–248.
[26] G. Bazzoni, E. Dejana, Endothelial cell-to-cell junctions: molecular organization and role in vascular homeostasis, Physiol. Rev. 84 (2004) 869–901.
[27] S.A. Figley, R. Khosravi, J.M. Legasto, Y.F. Tseng, M.G. Fehlings, Characterization of vascular disruption and blood-spinal cord barrier permeability following traumatic spinal cord injury, J. Neurotrauma 31 (2014) 541–552.
[28] Y.L. Jing, F. Bai, H. Chen, H. Dong, Meliorating microcirculatory with melatonin in rat model of spinal cord injury using laser Doppler flowmetry, Neuroreport 27 (2016) 1248–1255.
[29] M. Roustit, C. Millet, S. Blaise, B. Dufournet, J.L. Cracowski, Excellent reproducibility of laser speckle contrast imaging to assess skin microvascular reactivity, Microvasc. Res. 80 (2010) 505–511.
[30] M. Rossi, A. Carpi, F. Galetta, F. Franzoni, G. Santoro, The investigation of skin blood flowmotion: a new approach to study the microcirculatory impairment in vascular diseases? Biomed. Pharmacother. 60 (2006) 437–442.
[31] H.M. Stauss, Identification of blood pressure control mechanisms by power spectral analysis, Clin. Exp. Pharmacol. Physiol. 34 (2007) 362–368.
[32] H.M. Stauss, Power spectral analysis in mice: what are the appropriate frequency bands? Am. J. Phys. Regul. Integr. Comp. Phys. 292 (2007) (R902-R3).
[33] C.J. Boos, G.Y.H. Lip, A.D. Blann, Circulating endothelial cells in cardiovascular disease, J. Am. Coll. Cardiol. 48 (2006) 1538–1547.
[34] A.D. Blann, A. Woywodt, F. Bertolini, T.M. Bull, J.P. Buyon, R.M. Clancy, et al., Circulating endothelial cells - biomarker of vascular disease, Thromb. Haemost. 93 (2005) 228–235.
[35] F. Sabatier, L. Camoin-Jau, F. Anfosso, J. Sampol, F. Dignat-George, Circulating endothelial cells, microparticles and progenitors: key players towards the definition of vascular competence, J. Cell. Mol. Med. 13 (2009) 454–471.
[36] L. Giusti, D. Lucchesi, M. Garofolo, V.S. Bornez, G. Daniele, A. Dardano, et al., Factors affecting circulating endothelial progenitor cells (EPCs) and endothelial microparticles (EdMPs) in patients with type 2 diabetes, Diabetes 66 (2017) A593-A.
[37] J.L. Mehta, J. Szwedo, Circulating endothelial progenitor cells, microparticles and vascular disease, J. Hypertens. 28 (2010) 1611–1613.
[38] N. Kamei, S.M. Kwon, A. Kawamoto, M. Ii, M. Ishikawa, M. Ochi, et al., Contribution of bone marrow-derived endothelial progenitor cells to neovascularization and astrogliosis following spinal cord injury, J. Neurosci. Res. 90 (2012) 2281–2292.
[39] E. Paczkowska, D. Roginska, E. Pius-Sadowska, A. Jurewicz, K. Piecyk, K. Safranow, et al., Evidence for proangiogenic cellular and humoral systemic response in patients with acute onset of spinal cord injury, J Spinal Cord Med. 38 (2015) 729–744.
[40] P. Mancuso, I. Martin-Padura, A. Calleri, P. Marighetti, J. Quarna, C. Rabascio, et al., Circulating perivascular progenitors: a target of PDGFR inhibition, Int. J. Cancer 129 (2011) 1344–1350.
[41] N. Kamei, S.M. Kwon, A. Kawamoto, M. Ii, M. Ishikawa, M. Ochi, et al., Contribution of bone marrow-derived endothelial progenitor cells to neovascularization and astrogliosis following spinal cord injury, J. Neurosci. Res. 90 (2012) 2281–2292.
[42] H.M. Bramlett, W.D. Dietrich, Progressive damage after brain and spinal cord injury: pathomechanisms and treatment strategies, Prog. Brain Res. 161 (2007) 125–141.
[43] J.C. Fleming, M.D. Norenberg, D.A. Ramsay, G.A. Dekaban, A.E. Marcillo, A.D. Saenz, et al., The cellular inflammatory response in human spinal cords after injury, Brain 129 (2006) 3249–3269.
[44] D.H. Schweitzer, M.O. Vanderuit, G. Vanderpluijm, C.W.G.M. Lowik, S.E. Papapoulos, Interleukin-6 and the acute-phase response during treatment of patients with Pagets-disease with the nitrogen-containing bisphosphonate Dimethylaminohydroxypropylidene bisphosphonate, J. Bone Miner. Res. 10 (1995) 956–962.
[45] C.F. Hung, K.L. Mittelsteadt, R. Brauer, B.L. McKinney, T.S. Hallstrand, W.C. Parks, et al., Lung pericyte-like cells are functional interstitial immune sentinel cells, Am. J. Phys. Lung Cell. Mol. Phys. 312 (2017) (L556-L67).
[46] F.R. Jirik, T.J. Podor, T. Hirano, T. Kishimoto, D.J. Loskutoff, D.A. Carson, et al., Bacterial lipopolysaccharide and inflammatory mediators augment IL-6 secretion by human endothelial cells, J. Immunol. 142 (1989) 144–147.
[47] T. Naka, N. Nishimoto, T. Kishimoto, The paradigm of IL-6: from basic science to medicine, Arthritis Res. 4 (Suppl. 3) (2002) S233–S242.
[48] B. Schobitz, G. Pezeshki, T. Pohl, U. Hemmann, P.C. Heinrich, F. Holsboer, et al., Soluble interleukin-6 (IL-6) receptor augments central effects of IL-6 in vivo, FASEB J. 9 (1995) 659–664.
[49] B.S. Bochner, D.A. Klunk, S.A. Sterbinsky, R.L. Coffman, R.P. Schleimer, IL-13 selectively induces vascular cell adhesion molecule-1 expression in human endothelial cells, J. Immunol. 154 (1995) 799–803.
[50] C.Y. Chang, J.R. Li, Y.C. Ou, S.Y. Lin, Y.Y. Wang, W.Y. Chen, et al., Interplay of inflammatory gene expression in pericytes following Japanese encephalitis virus infection, Brain Behav. Immun. 66 (2017) 230–243.
[51] K. Leghmari, Y. Bennasser, E. Bahraoui, HIV-1 Tat protein induces IL-10 production in monocytes by classical and alternative NF-kappaB pathways, Eur. J. Cell Biol. 87 (2008) 947–962.
[52] T. Rubic, R.L. Lorenz, Downregulated CD36 and oxLDL uptake and stimulated ABCA1/G1 and cholesterol efflux as anti-atherosclerotic mechanisms of interleukin-10, Cardiovasc. Res. 69 (2006) 527–535.
[53] J. Li, Y. Zou, J. Ge, D. Zhang, A. Guan, J. Wu, et al., The effects of G-CSF on proliferation of mouse myocardial microvascular endothelial cells, Int. J. Mol. Sci. 12 (2011) 1306–1315.
[54] K.W. Park, Y.W. Kwon, H.J. Cho, J.I. Shin, Y.J. Kim, S.E. Lee, et al., G-CSF exerts dual effects on endothelial cells–opposing actions of direct eNOS induction versus indirect CRP elevation, J. Mol. Cell. Cardiol. 45 (2008) 670–678.
[55] J. Su, H. Zhou, Y. Tao, J. Guo, Z. Guo, S. Zhang, et al., G-CSF protects human brain vascular endothelial cells injury induced by high glucose, free fatty acids and hypoxia through MAPK and Akt signaling, PLoS One 10 (2015) e0120707.